Fundamental constraints on the strength of transition-metal borides: The case of CrB_4

Bing Li,[1] Hong Sun,[1,*] Chenpeng Zang,[1] and Changfeng Chen[2,†]

[1]*Department of Physics and Key Laboratory of Artificial Structures and Quantum Control (Ministry of Education), Shanghai Jiao Tong University, Shanghai 200240, China*

[2]*Department of Physics and High Pressure Science and Engineering Center, University of Nevada, Las Vegas, Nevada 89154, USA*

(Received 7 April 2013; published 20 May 2013)

Recent theoretical calculations predict an ideal shear strength over 50 GPa for CrB_4, placing it well above ultrahard ReB_2 in terms of strength and thus suggesting possible superhardness of CrB_4. This result, however, is contradicted by the latest experimental measurements that produced a relatively low Vickers hardness around 23 GPa, which is about the same as the hardness value of ReB_2. To solve this intriguing problem, we have performed a systematic first-principles study that unveils two fundamental constraints that limit the strength of CrB_4: (i) a quantum-mechanical effect involving a transition between two-center and three-center bonding among the boron atoms that reduces the rigidity and directionality of the boron bonding and (ii) a mechanistic effect caused by the pressure beneath the indenter that drives a lateral bond and volume expansion that further stretches and weakens the boron bonds in addition to the shear deformation in the CrB_4 structure under Vickers indentation hardness tests. These effects lead to considerably reduced strength of CrB_4, producing an ideal (i.e., an upper bound) indentation strength of 27 GPa that is consistent with the experimental results. These constraints also explain previous results on the pure shear and indentation strength for ReB_2, WB_3, and MoB_3, limiting their ideal (Vickers) indentation strength below 30 GPa irrespective of the composition and structural details. The present results suggest that transition-metal boron compounds are unlikely to become superhard as previously predicted.

DOI: 10.1103/PhysRevB.87.174106 PACS number(s): 62.20.−x, 81.40.Jj, 61.50.Ah

I. INTRODUCTION

Recent success in synthesizing rhenium diboride (ReB_2)[1] at ambient pressure has reignited great interest in studying this class of ultraincompressible and ultrahard materials consisting of small, light covalent elements (B, C, N) with large, electron-rich transition metals (Cr, Mn, Ru, W, Re, Os, etc.). These materials provide a low-cost alternative to traditional superhard materials like diamond and cubic boron nitride that require high-temperature and high-pressure synthesis conditions. The covalent elements can form strong and directional covalent bonds with the transition metals, while the high density of valence electrons from the transition metals prevents the lattice structures from being squeezed together, both of which enhance the resistance of the transition-metal light-element compounds against large plastic (bulk and shear) deformation and lead to increased hardness. Various transition-metal light-element compounds have been successfully synthesized, among which transition-metal boron (TM-B) compounds, such as OsB_2,[2] ReB_2,[1,3–7] RuB_2,[5] WB_4,[5,8–10] and CrB_4,[11,12] attracted special attention for their high hardness due to their high content of boron. While there is still controversy concerning the structural assignment of synthesized WB_4,[13,14] the structure of CrB_4 has recently been clarified[11,12] where tilted boron cages surrounding each Cr atom connected by strong B-B bonds form a three-dimensional (3D) boron network. Such a structure is expected to exhibit superrigidity and enhance the hardness of CrB_4. Theoretical calculations predict that the ideal shear strength, which is closely related to material hardness, of CrB_4 would reach 51 GPa,[11] which is much higher than that of ReB_2 (35 GPa),[15] which has a structure of buckled two-dimensional (2D) boron layers separated by large Re atoms. However, the latest experimental measurements show that the asymptotic Vickers hardness of CrB_4 (23.3 GPa)[12] is only comparable to, if not lower than, that of ReB_2 (30.1, 26.6, 18.4 GPa).[1,5,6] This contrasting result raises several important questions: How do boron content and different boron network structures in TM-B compounds influence their hardness? How can the (Vickers) hardness of TM-B compounds be accurately predicted based on first-principles calculations? Most importantly, can TM-B compounds become superhard with (Vickers) hardness exceeding 40 GPa?

Recent advances in computation physics have made it possible to calculate the stress-strain relations of a perfect crystal in various shear deformation directions under the normal compressive pressure beneath an indenter. The lowest shear peak stress under an indenter, which is defined as the ideal indentation strength, gives the stress at which a perfect crystal becomes mechanically unstable under indentation.[15–18] Ideal indentation strength provides a more accurate description of a material's strength under indentation hardness tests than pure ideal shear strength that is calculated neglecting the normal pressure beneath the indenter.[19–29] While material strength and hardness are controlled by many factors, such as defect nucleation and mobility, ideal shear (indentation) strength calculations can predict incipient plasticity in a crystal[30] and determine the lowest shear stress needed to destabilize a perfect crystal, thus setting an upper bound for material strength. The measured strength of high-quality samples can actually approach the calculated ideal strength.[31,32] This makes ideal shear (indentation) strength a benchmark quantity in assessing material strength and hardness; it is especially useful in a comparative study of different materials. Previous ideal shear strength calculations for CrB_4 were carried out only on simple {100} crystalline planes without considering the normal pressure beneath the indenter, which produced a high ideal shear strength of 51 GPa.[11] In this paper, we report on a systematic study of the ideal strength of CrB_4 under different loading conditions. We first perform a more comprehensive set of calculations to determine the pure ideal shear strength, and our results reveal a significant reduction stemming from

TABLE I. The calculated lattice constants a, b, and c (Å), bulk (B) and shear (G) moduli (GPa), and Poisson's ratio ν, as well elastic constants C_{ij} (GPa) for CrB_4 compared with previous calculations and available experiment results.

	a	b	c		B	G	ν	
	4.723	5.474	2.851		263	267	0.121	
	4.725	5.476	2.847[a]		265	261[a]		
	4.726	5.474	2.850[b]					
C_{11}	C_{22}	C_{33}	C_{12}	C_{13}	C_{23}	C_{44}	C_{55}	C_{66}
542	855	492	50	104	87	252	280	253
554	880	473	65	107	95	254	282	250[a]

[a]Reference 11.
[b]Reference 12.

the intriguing ability of boron atom to form both two-center and three-center bonding that leads to new deformation paths along certain shear directions that were not examined in previous studies. We also carried out calculations of the ideal (Vickers) indentation strength of CrB_4 and obtained a value of 27.6 GPa, which is in good agreement with the experimental value (23.3 GPa).[12] A detailed analysis of the bond-breaking processes of CrB_4 structure under indentation shear deformation illustrates that the uniaxial normal compressive pressure beneath the indenter can cause a large lateral volume expansion which further stretches and weakens the boron atomic bonds in addition to that caused by the shear deformation. Similar phenomena have been observed in other TM-B compounds with different boron content and structure, such as ReB_2, WB_3, and MoB_3, limiting their indentation strength to below 30 GPa.[14,15] These results suggest that it is unlikely that TM-B compounds can be superhard, with the Vickers hardness exceeding 40 GPa, as previously thought.

II. COMPUTATIONAL METHOD

We performed calculations of ideal pure shear and indentation strength under a Vickers indenter using the VASP code[33] and adopting the projector augmented wave (PAW) potentials[34] with the semicore $3p$ electron states of Cr treated as valence electrons and the generalized gradient approximation (GGA) for the exchange-correlation energy with a plane-wave basis set. The GGA-PBE exchange-correlation functional proposed by Perdew, Burke, and Ernzerhof (PBE)[35] was used. The total energy of the structure was minimized by relaxing the structural parameters using a conjugate gradient optimization method.[36] The total-energy and stress calculations used an orthorhombic unit cell with space group *Pnnm* (No. 58) for CrB_4 determined previously.[11,12] A $9 \times 9 \times 11$ Monkhorst-Pack[37] k-point grid and a 600-eV energy cutoff were used in the calculations. The energy convergence of the

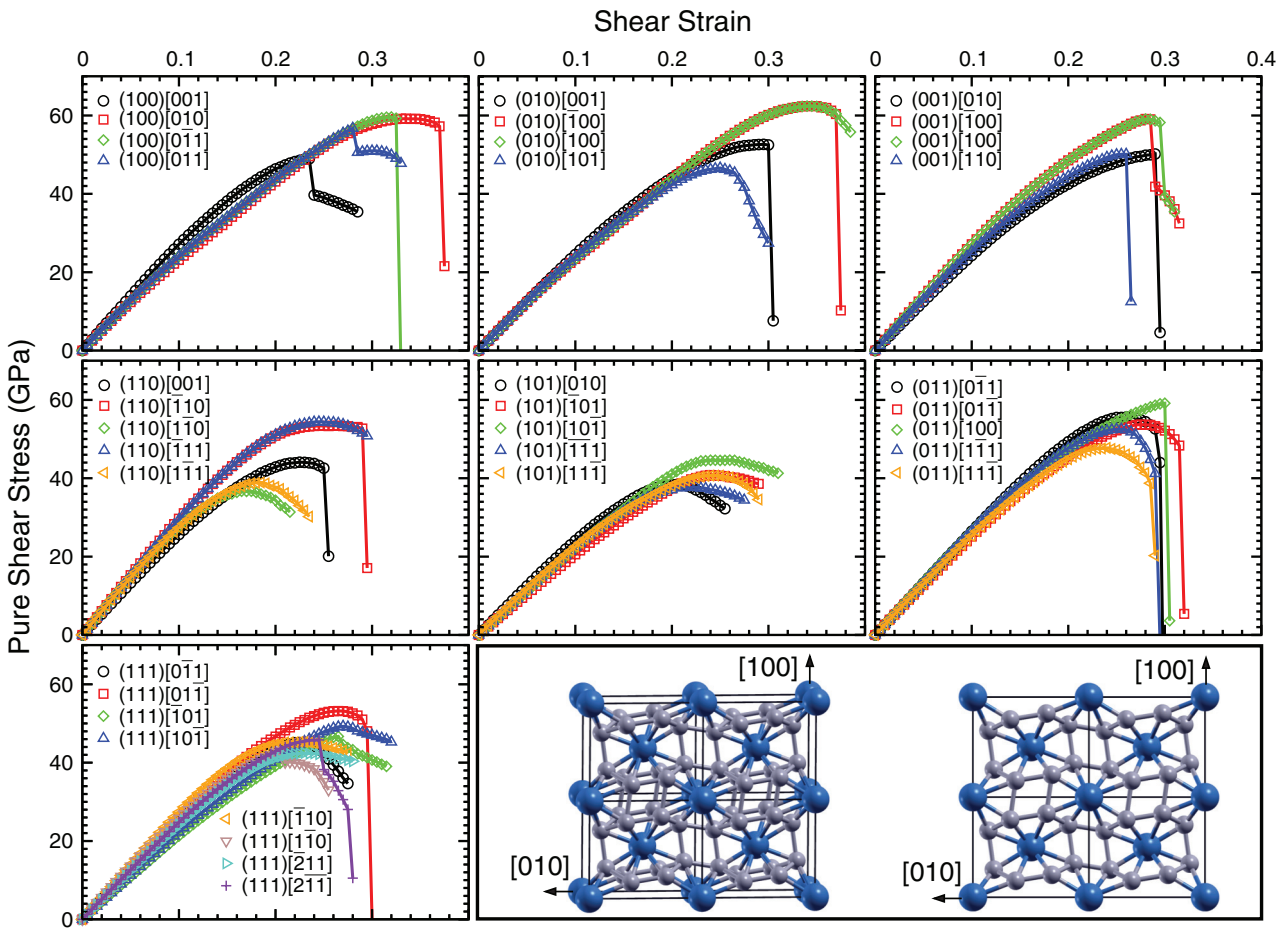

FIG. 1. (Color online) The calculated stress-strain curves on various shear sliding planes in different directions under pure shear deformation for CrB_4. Also given are the $2 \times 2 \times 1$ supercell of CrB_4 and its front view.

calculation is on the order of 1 meV per atom, with the residual stresses and forces in the fully relaxed structures less than 0.1 GPa and 0.001 eV/Å. The spin-polarized calculations were tried first with no magnetic moment found for CrB_4, consistent with the previous results,[11] so all the calculations were carried out using non-spin-polarized calculations. The quasistatic ideal indentation strength and relaxed loading path were determined using a method described previously.[15–18] In this method, the shape of the (deformed) unit cell, the positions of the atoms, and the relation between the shear stress σ_{xz} and shear strain ϵ_{xz} are determined completely at each step following a constrained atomic relaxation procedure, including the effect of the normal compressive pressure σ_{zz} by requiring that $\sigma_{zz} = \sigma_{xz} \tan \Phi$ at each deformation step, with Φ being the center-line–to–face angle of the Vickers indenter. The lowest peak stress in all the indentation shear directions determines the ideal indentation strength of the structure, at which the crystal structure starts to destabilize under the indenter. In a special case of setting $\sigma_{zz} = 0$, we recover the normal relaxation procedure used in previous calculations of pure ideal shear stresses[19–29] that neglect the effects of the normal compressive pressure beneath the indenter. As a test, we performed calculations for the equilibrium structures of CrB_4, and the obtained results for the elastic constants, bulk and shear moduli, and Poisson's ratios (see Table I) are all in good agreement with the previously reported experimental and calculated results.[11,12]

III. RESULTS AND DISCUSSION

We plot in Fig. 1 the calculated stress-strain curves on various shear sliding planes in different inequivalent directions under pure shear deformation for CrB_4. On the simple {100} planes the peak stresses in all directions are indeed high ($\geqslant$50 GPa), in agreement with the results of previous calculations.[11] However, on the {110} planes, the pure shear peak stresses are much reduced, with the lowest peak stress of 36.7 GPa appearing in the $(110)[1\bar{1}0]$ shear direction. This value is just slightly higher than the lowest pure shear stress peak (35.3 GPa)[15] of ReB_2. In Fig. 2, we show the calculated stress-strain curves on various shear sliding planes in different inequivalent directions under (Vickers) indentation shear deformations for CrB_4. The obtained values on all crystalline planes are lower than 40 GPa, with the lowest peak (27.6 GPa) appearing in the (100)[001] direction. This ideal indentation strength value is the same as that (27.6 GPa) of ReB_2.[15] The reduction of the shear strength of CrB_4 in the (100)[001] direction due to the normal compressive pressure in the Vickers indentation is more than 40%. In Table II, we list all the calculated peak stresses and corresponding strains for CrB_4 in various directions under pure (σ_m^p and ϵ_m^p) and Vickers (σ_m^V and ϵ_m^V) shear deformation. In Table III, we give the calculated lowest peak stresses and corresponding strains on different crystalline planes for CrB_4 under pure (σ_m^p and ϵ_m^p) and Vickers

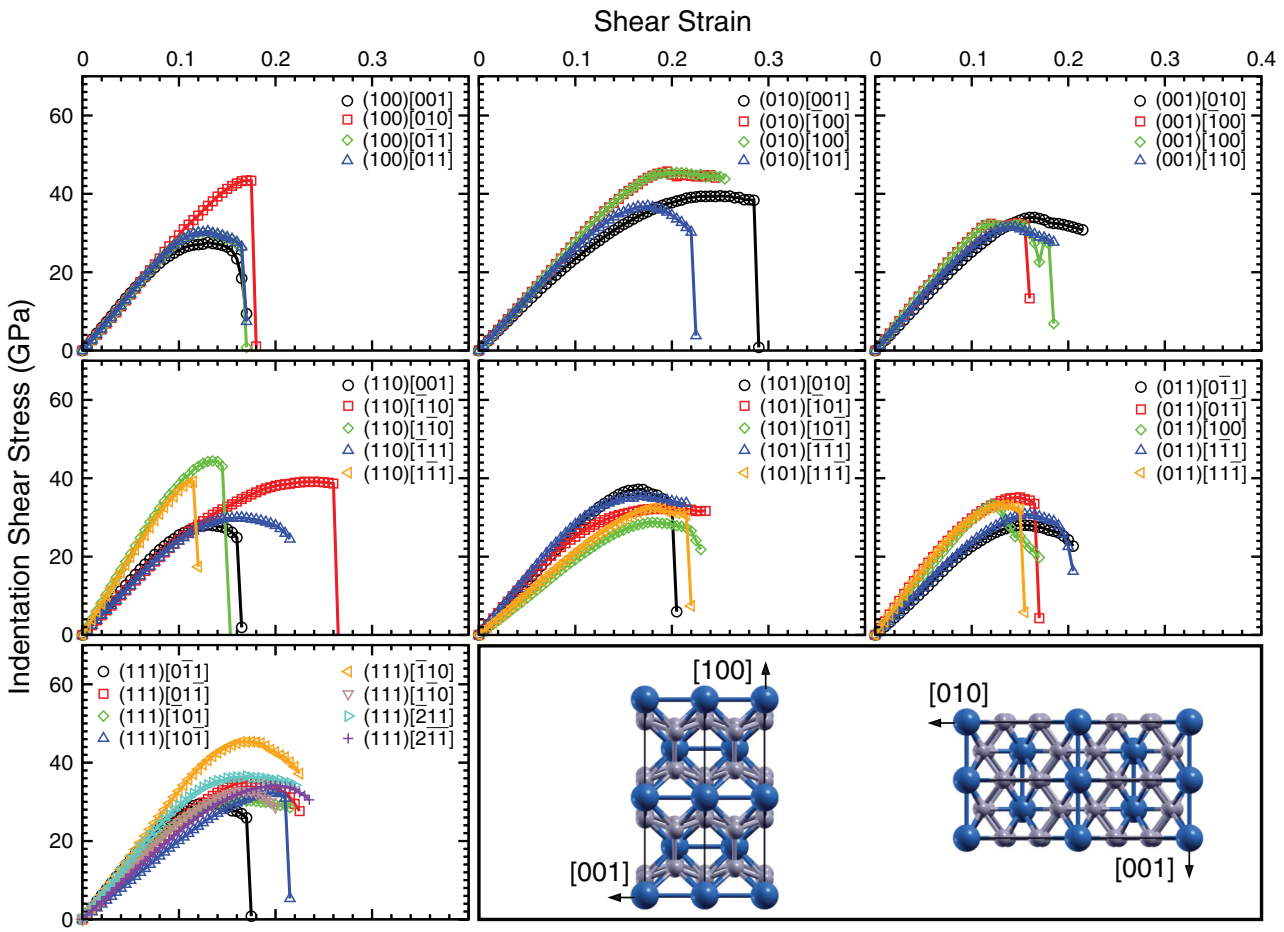

FIG. 2. (Color online) The calculated stress-strain curves on various shear sliding planes in different directions under Vickers shear deformation for CrB_4. Also given are the side and top views of the supercell of CrB_4 (see Fig. 1).

TABLE II. The calculated peak stresses (GPa) and corresponding strains for CrB_4 in various directions under pure (σ_m^p and ϵ_m^p) and Vickers (σ_m^V and ϵ_m^V) shear deformation.

Shear	σ_m^p	ϵ_m^p	σ_m^V	ϵ_m^V	Shear	σ_m^p	ϵ_m^p	σ_m^V	ϵ_m^V	Shear	σ_m^p	ϵ_m^p	σ_m^V	ϵ_m^V
(100)[001]	49.0	0.230	27.6	0.125	(010)[001]	52.6	0.290	39.5	0.245	(001)[010]	50.2	0.285	34.0	0.160
(100)[010]	59.2	0.330	43.4	0.155	(010)[$\bar{1}$00]	62.4	0.335	45.7	0.190	(001)[$\bar{1}$00]	59.1	0.275	32.4	0.140
(100)[0$\bar{1}$1]	59.6	0.315	30.3	0.125	(010)[100]	62.4	0.335	45.5	0.200	(001)[100]	59.1	0.275	32.3	0.145
(100)[011]	56.7	0.275	30.4	0.125	(010)[101]	46.6	0.295	36.9	0.170	(001)[110]	50.1	0.255	31.6	0.130
(110)[001]	44.1	0.220	28.1	0.125	(101)[010]	38.4	0.200	37.2	0.160	(011)[0$\bar{1}$1]	55.6	0.260	28.0	0.150
(110)[$\bar{1}$10]	53.4	0.255	39.1	0.235	(101)[$\bar{1}$01]	40.8	0.235	32.2	0.180	(011)[01$\bar{1}$]	53.7	0.270	35.1	0.145
(110)[1$\bar{1}$0]	36.7	0.160	44.4	0.130	(101)[10$\bar{1}$]	44.6	0.255	28.7	0.175	(011)[100]	59.1	0.295	33.4	0.115
(110)[$\bar{1}$11]	54.4	0.240	30.0	0.160	(101)[$\bar{1}\bar{1}$1]	37.7	0.220	35.5	0.160	(011)[1$\bar{1}$1]	52.5	0.250	30.8	0.150
(110)[1$\bar{1}$1]	38.9	0.180	39.1	0.110	(101)[11$\bar{1}$]	40.7	0.235	32.4	0.175	(011)[11$\bar{1}$]	47.8	0.235	33.2	0.130
(111)[0$\bar{1}$1]	45.1	0.220	29.6	0.120	(111)[01$\bar{1}$]	53.2	0.260	35.0	0.170	(111)[$\bar{1}$01]	46.7	0.260	30.4	0.160
(111)[10$\bar{1}$]	49.3	0.265	32.3	0.190	(111)[$\bar{1}$10]	45.3	0.220	45.3	0.170	(111)[1$\bar{1}$0]	43.1	0.200	32.8	0.160
(111)[$\bar{2}$11]	42.5	0.225	36.6	0.165	(111)[2$\bar{1}\bar{1}$]	45.8	0.340	34.2	0.190					

(σ_m^V and ϵ_m^V) shear deformation, together with the difference of the lowest peak stresses [$\Delta\sigma_m = (\sigma_m^p - \sigma_m^V)/\sigma_m^p$]. The strength reductions by the normal compressive pressures beneath indenters are fairly large (−20% to about −60%).

To analyze the bond-breaking mechanism of CrB_4 in its weakest pure shear deformation direction (110)[1$\bar{1}$0], we plot in Fig. 3 the calculated structural snapshots of CrB_4 at equilibrium ($\epsilon = 0$) and in the (110)[1$\bar{1}$0] direction under pure shear at strains $\epsilon = 0.125$ and $\epsilon = 0.17$, together with the 3D electron localization function (ELF) isosurfaces, which gives a local measurement of electron paring,[38] at ELF = 0.73. Also plotted in Fig. 3 are the 2D ELF on the (001) planes passing through the boron atoms (B_1–B_4) indicated by the circles. We track the bonding changes of these four boron atoms (B_1–B_4) to understand the deformation pattern of CrB_4 in the weakest (110)[1$\bar{1}$0] direction under pure shear. At the equilibrium ($\epsilon = 0$), the lengths of the atomic bonds $|B_1\text{-}B_2| = |B_3\text{-}B_4|$ (1.732 Å) and $|B_2\text{-}B_3| = |B_1\text{-}B_4|$ (1.851 Å) are both shorter than that of $|B_2\text{-}B_4|$ (2.129 Å). Here, two-center covalent boron bonds form between B_1-B_2, B_2-B_3, B_3-B_4, and B_4-B_1, as illustrated by the 3D ELF isosurfaces or 2D ELF plot (left panels of Fig. 3). As the shear deformation increases in the (110)[1$\bar{1}$0] direction, the bond lengths of $|B_2\text{-}B_3|$ and $|B_1\text{-}B_4|$ increase, which induces a charge transfer from the B_2-B_3 and B_1-B_4 bonds to the centers of $\triangle B_1B_2B_4$ and $\triangle B_2B_3B_4$, forming three-center bonds,[29] and then to the B_1-B_2 and B_3-B_4 bonds as the shear strain further increases (middle and right panels of Fig. 3). Such three-center bonding-mediated structural transformations have been found in γ-B_{28}[29] and MoB_3.[14] This intriguing quantum effect that gives boron atoms the ability to form three-center bonding configurations plays a key role in reducing considerably the potential barriers and therefore the shear strength of boron-rich materials under shear deformations. It allows charge to transfer continuously without the usual hard bond breaking in strong covalent solids such as diamond and cubic BN,[39,40] and it makes a smooth transition from one two-center covalent bond (for instance, B_2-B_3 and B_1-B_4 in CrB_4) to a new two-center covalent bond (for instance, B_1-B_2 and B_3-B_4 in CrB_4), resulting in much reduced rigidity and directionality of the boron covalent bonds.

TABLE III. The calculated lowest peak stresses (GPa) and corresponding strains on different crystalline planes for CrB_4 under pure (σ_m^p and ϵ_m^p) or Vickers (σ_m^V and ϵ_m^V) shear deformation, together with the difference of the lowest peak stresses [$\Delta\sigma_m = (\sigma_m^p - \sigma_m^V)/\sigma_m^p$].

Pure	σ_m^p	ϵ_m^p	Vickers	σ_m^V	ϵ_m^V	$\Delta\sigma_m$
(100)[001]	49.0	0.230	(100)[001]	27.6	0.125	−43.7%
(010)[101]	46.6	0.295	(010)[101]	36.9	0.170	−20.8%
(001)[110]	50.1	0.255	(001)[110]	31.6	0.130	−58.5%
(110)[1$\bar{1}$0]	36.7	0.160	(110)[001]	28.1	0.125	−23.4%
(101)[$\bar{1}\bar{1}$1]	37.7	0.220	(101)[10$\bar{1}$]	28.7	0.175	−23.9%
(011)[1$\bar{1}$1]	52.5	0.250	(011)[0$\bar{1}$1]	28.0	0.150	−46.7%
(111)[$\bar{2}$11]	42.5	0.225	(111)[0$\bar{1}$1]	29.6	0.120	−30.4%

The large reduction of shear strength in CrB_4 under the (Vickers) indentation shear deformation has a different and more mechanistic mechanism. In Fig. 4 we plot the calculated structural snapshots of CrB_4 at equilibrium ($\epsilon = 0$) and in the weakest indentation shear direction (100)[001] at $\epsilon = 0.15$ under both Vickers indentation and pure shear deformations, together with the 3D ELF isosurfaces at ELF = 0.73. Also shown in Fig. 4 are the 2D ELF on the (100) planes passing through the upper layer of boron atoms indicated by the circles. In CrB_4, boron atoms form two buckled boron layers parallel to the (100) plane in one unit cell (see the side view of the CrB_4 supercell in Fig. 2). At equilibrium ($\epsilon = 0$), the boron atoms form buckled hexagonal covalent bonding rings on the (100) planes (left panels of Fig. 4). Under indentation shear deformation in the (100)[001] direction, the normal compressive pressure beneath the indenter induces a lateral expansion of the volume with the lattice constants b and c increasing from 5.474 and 2.851 Å at $\epsilon = 0$ to 5.607 and 3.089 Å at $\epsilon = 0.15$, respectively, after passing the indentation peak stress (see Fig. 2), which causes the stretching and eventually breaking up of some covalent boron bonds in the (100) hexagonal rings, for instance, the B_3-B_5 and B_4-B_6 bonds, as shown in the middle panels of Fig. 4. While under pure shear, the lateral expansion does not exist ($b = 5.470$ Å and $c = 2.840$ Å at $\epsilon = 0.15$), and the covalent boron bonds in the (100) hexagonal rings remain intact under the same shear strain ($\epsilon = 0.15$; right panels of Fig. 4). In fact, under the (100)[001] pure shear, the structure of CrB_4 remains stable when $\epsilon < 0.23$ (see Fig. 1 and Table II). Such lateral

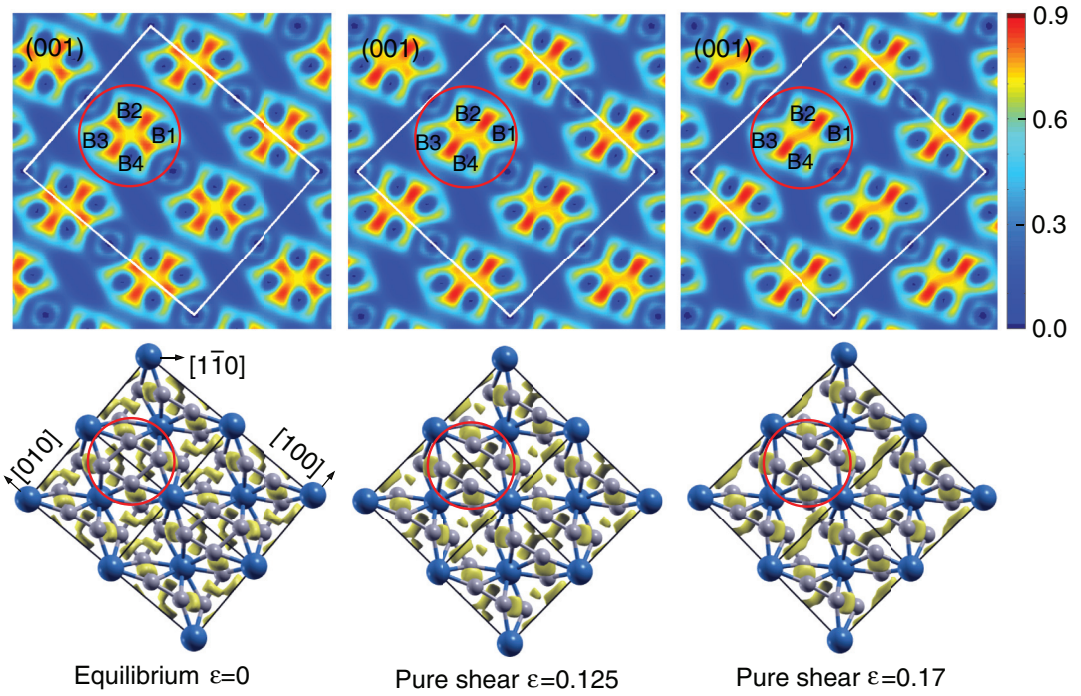

FIG. 3. (Color online) The calculated structural snapshots of CrB_4 at equilibrium ($\epsilon = 0$) and in the (110)[1$\bar{1}$0] shear direction under pure shear ($\epsilon = 0.125$ and $\epsilon = 0.17$), with the three-dimensional ELF isosurfaces at ELF = 0.73. Also shown are the two-dimensional ELF on the (001) planes passing through the boron atoms indicated by the circles.

expansion-induced boron bond early breaking under (Vickers) indentation shear deformation has been found in ReB_2,[15] WB_3, and MoB_3,[14] limiting the indentation strength of these TM-B compounds to below 30 GPa.

In Fig. 5, we present the calculated total density of states and the partial density of states (PDOS) of CrB_4 at equilibrium [$\epsilon = 0$; Fig. 5(a)] and in the (100)[001] shear direction under Vickers indentation shear at $\epsilon = 0.15$ [Fig. 5(b)]. The PDOSs of B atoms in the unit cell are divided into two identical groups, while those of Cr atoms are the same. At equilibrium ($\epsilon = 0$), the calculated total DOS and PDOS agree well with the previous calculations,[11] where in the range of (−10, −5) eV B s and B p states combine to form hybrid sp^3 boron bonds that form a 3D boron network; in the range of (−5, −2) eV B p_y (p_z) and Cr d_{xy} (d_{xz}) states combine to form strong covalent Cr-B bonds, and in the range of (−2, 0) eV Cr $d_{x^2-y^2}$ and Cr d_{yz} states form

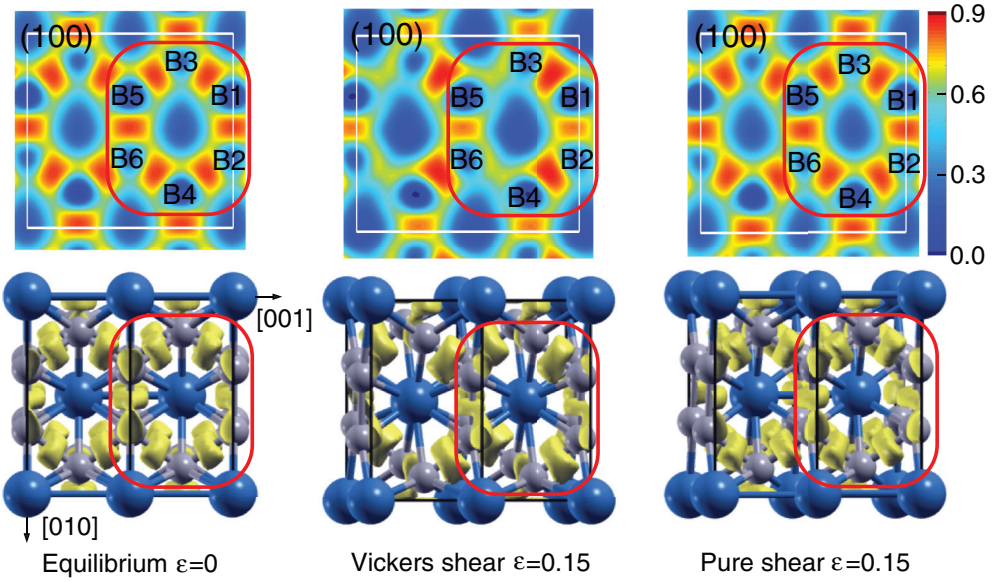

FIG. 4. (Color online) The calculated structural snapshots of CrB_4 at equilibrium ($\epsilon = 0$) and in the (100)[001] shear direction under Vickers and pure shear ($\epsilon = 0.15$) with the three-dimensional ELF isosurfaces at ELF = 0.73. Also shown are the two-dimensional ELF on the (100) planes passing through the upper layer of boron atoms indicated by the circles.

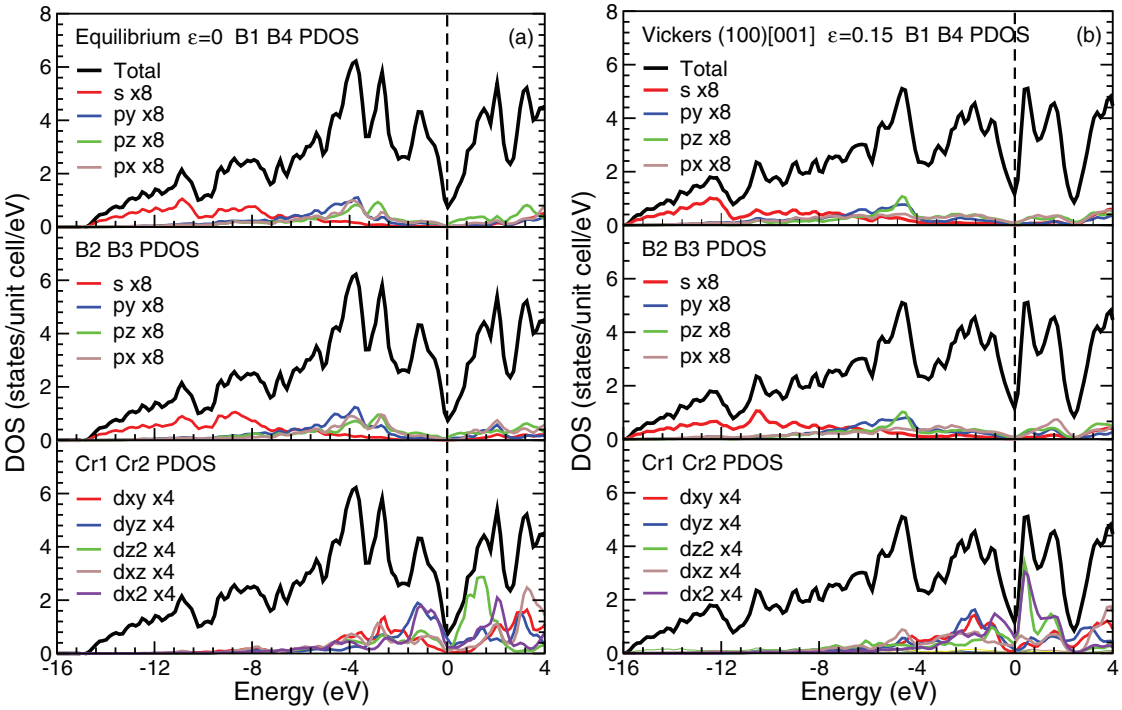

FIG. 5. (Color online) The calculated total and partial DOS of CrB_4 (a) at equilibrium ($\epsilon = 0$) and (b) in the (100)[001] Vickers shear direction ($\epsilon = 0.15$) with E_F at $E = 0$. The partial DOSs of B atoms in the unit cell are divided into two identical groups, while those of Cr atoms are the same.

the nonbonding states, above which lies the Fermi energy E_F at the bottom of a pseudogap. In the weakest indentation shear direction (100)[001] at $\epsilon = 0.15$ after passing the indentation peak stress (see Fig. 2), the following changes in the PDOS are observed: the B s states in the range of $(-10, -5)$ eV are reduced, which makes the coupling between the B s and B p states weaker, indicating the boron bond-breaking processes depicted in the middle panels of Fig. 4; the Cr d_{xy} states move to higher energy, which reduces their hybridization with the B p states due to the lateral expansion of the unit cell in b and c under the normal compressive pressure beneath the indenter. These changes in the PDOS of CrB_4 electronic states under indentation shear deformation are consistent with the deformation patterns shown in Fig. 4.

IV. CONCLUSIONS

We have performed systematic first-principles calculations to examine the pure shear and indentation strength of CrB_4, which was predicted by previous calculations to be a potential superhard material but exhibited lower than expected hardness under indentation tests. Our results unveil two fundamental constraints that were not considered in earlier studies, and they limit the intrinsic strength of CrB_4, thus explaining the observed relatively low hardness result. The first constraint is of fundamental quantum nature, stemming from boron's ability to form both two-center and three-center atomic bonds, which lowers the barrier for the transition of bonding configurations in CrB_4 under structural deformation, leading to considerably reduced ideal shear strength. The second constraint is a mechanistic one imposed by the indentation process. The normal pressure beneath the indenter is transmitted effectively through the TM valence electrons, producing a large lateral volume expansion and resultant stretching and breaking of the boron bonds. Consequently, the high boron concentration and the 3D boron networks are not expected to enhance the strength of TM-B compounds like CrB_4 very much. Similar behaviors also have been observed in other TM-B compounds, including ReB_2,[15] WB_3,[14] and MoB_3,[14] limiting their ideal (Vickers) indentation strength to below 30 GPa, irrespective of the composition and structural details. These results suggest that TM-B compounds are unlikely to become superhard, with Vickers hardness exceeding 40 GPa.

ACKNOWLEDGMENTS

This work was supported by the DOE (Grant No. DE-FC52-06NA26274) at UNLV and NNSF of China (Grant No. 11174200) at SJTU. H.S. appreciates the support of the Science and Engineering Interdisciplinary Research Foundation of SJTU.

*Corresponding author: hsun@sjtu.edu.cn
†Corresponding author: chen@physics.unlv.edu

[1] H. Y. Chung, M. B. Weinberger, J. B. Levine, A. Kavner, J. M. Yang, S. H. Tolbert, and R. B. Kaner, Science **316**, 436 (2007).
[2] R. B. Kaner, J. J. Gilman, and S. H. Tolbert, Science **308**, 1268 (2005).
[3] J. B. Levine, S. L. Nguyen, H. I. Rasool, J. A. Wright, S. E. Brown, and R. B. Kaner, J. Am. Chem. Soc. **130**, 16953 (2008).

[4]A. Latini, J. V. Rau, D. Ferro, R. Teghil, V. R. Albertini, and S. M. Barinov, Chem. Mater. **20**, 4507 (2008).
[5]Q. Gu, G. Krauss, and W. Steurer, Adv. Mater. **20**, 3620 (2008).
[6]J. Q. Qin, D. W. He, J. H. Wang, L. M. Fang, L. Lei, Y. J. Li, J. A. Hu, Z. L. Kou, and Y. Bi, Adv. Mater. **20**, 4780 (2008).
[7]N. Orlovskaya, Z. L. Xie, M. Klimov, H. Heinrich, D. Restrepo, R. Blair, and C. Suryanarayana, J. Mater. Res. **26**, 2772 (2011).
[8]R. Mohammadi, A. T. Lech, M. Xie, B. E. Weaver, M. T. Yeung, S. H. Tolbert, and R. B. Kaner, Proc. Natl. Acad. Sci. USA **108**, 10958 (2011).
[9]C. Liu, F. Peng, N. Tan, J. Liu, F. Li, J. Qina, J. Wang, Q. Wang, and D. He, High Pressure Res. **31**, 275 (2011).
[10]M. Xie, R. Mohammadi, Z. Mao, M. M. Armentrout, A. Kavner, R. B. Kaner, and S. H. Tolbert, Phys. Rev. B **85**, 064118 (2012).
[11]H. Niu, J. Wang, X. Q. Chen, D. Li, Y. Li, P. Lazar, R. Podloucky, and A. N. Kolmogorov, Phys. Rev. B **85**, 144116 (2012).
[12]A. Knappschneider, C. Litterscheid, D. Dzivenko, J. A. Kurzman, R. Seshadri, N. Wagner, J. Beck, R. Riedel, and B. Albert, Inorg. Chem. **52**, 540 (2013).
[13]R. F. Zhang, D. Legut, Z. J. Lin, Y. S. Zhao, H. K. Mao, and S. Veprek, Phys. Rev. Lett. **108**, 255502 (2012).
[14]C. P. Zang, H. Sun, and C. F. Chen, Phys. Rev. B **86**, 180101(R) (2012).
[15]C. Zang, H. Sun, J. S. Tse, and C. Chen, Phys. Rev. B **86**, 014108 (2012).
[16]Z. C. Pan, H. Sun, and C. F. Chen, Phys. Rev. Lett. **98**, 135505 (2007).
[17]Z. C. Pan, H. Sun, and C. F. Chen, Phys. Rev. B **79**, 104102 (2009).
[18]Z. C. Pan, H. Sun, Y. Zhang, and C. F. Chen, Phys. Rev. Lett. **102**, 055503 (2009).
[19]D. Roundy, C. R. Krenn, M. L. Cohen, and J. W. Morris, Jr., Phys. Rev. Lett. **82**, 2713 (1999).
[20]H. Chacham and L. Kleinman, Phys. Rev. Lett. **85**, 4904 (2000).
[21]S. H. Jhi, S. G. Louie, M. L. Cohen, and J. W. Morris, Jr., Phys. Rev. Lett. **87**, 075503 (2001).
[22]S. Ogata, J. Li, and S. Yip, Science **298**, 807 (2002).
[23]D. M. Clatterbuck, C. R. Krenn, M. L. Cohen, and J. W. Morris, Jr., Phys. Rev. Lett. **91**, 135501 (2003).
[24]X. Blase, P. Gillet, A. San Miguel, and P. Mélinon, Phys. Rev. Lett. **92**, 215505 (2004).
[25]Y. Zhang, H. Sun, and C. F. Chen, Phys. Rev. Lett. **93**, 195504 (2004); **94**, 145505 (2005).
[26]M. G. Fyta, I. N. Remediakis, P. C. Kelires, and D. A. Papaconstantopoulos, Phys. Rev. Lett. **96**, 185503 (2006).
[27]J. Yang, H. Sun, and C. F. Chen, J. Am. Chem. Soc. **130**, 7200 (2008).
[28]P. Lazar, X. Q. Chen, and R. Podloucky, Phys. Rev. B **80**, 012103 (2009).
[29]W. Zhou, H. Sun, and C. F. Chen, Phys. Rev. Lett. **105**, 215503 (2010).
[30]J. Li, K. J. Van Vliet, T. Zhu, S. Yip, and S. Suresh, Nature (London) **418**, 307 (2002).
[31]A. Gouldstone, H.-J. Koh, K.-Y. Zeng, A. E. Giannakopoulos, and S. Suresh, Acta Mater. **48**, 2277 (2000).
[32]C. R. Krenn, D. Roundy, M. L. Cohen, D. C. Chrzan, and J. W. Morris, Jr., Phys. Rev. B **65**, 134111 (2002).
[33]See http://www.vasp.at/.
[34]P. E. Blöchl, Phys. Rev. B **50**, 17953 (1994); G. Kresse and D. Joubert, *ibid.* **59**, 1758 (1999).
[35]J. P. Perdew, K. Burke, and M. Ernzerhof, Phys. Rev. Lett. **77**, 3865 (1996).
[36]M. P. Teter, M. C. Payne, and D. C. Allan, Phys. Rev. B **40**, 12255 (1989); D. M. Bylander, L. Kleinman, and S. Lee, *ibid.* **42**, 1394 (1990).
[37]H. J. Monkhorst and J. D. Pack, Phys. Rev. B **13**, 5188 (1976).
[38]A. D. Becke and K. E. Edgecombe, J. Chem. Phys. **92**, 5397 (1990); B. Silvi and A. Savin, Nature (London) **371**, 683 (1994).
[39]Y. Zhang, H. Sun, and C. F. Chen, Phys. Rev. B **73**, 144115 (2006).
[40]Y. Zhang, H. Sun, and C. F. Chen, Phys. Rev. B **73**, 064109 (2006).